Applied Physics Letters

# Utilizing time domain electrical methods to monitor MLCCs' degradation

Cite as: Appl. Phys. Lett. **122**, 112902 (2023); https://doi.org/10.1063/5.0138806
Submitted: 14 December 2022 • Accepted: 27 February 2023 • Published Online: 13 March 2023

Pedram Yousefian, Shalini Rajpoot and Clive A. Randall







AIP Publishing

Applied Physics Letters ARTICLE scitation.org/journal/apl

# Utilizing time domain electrical methods to monitor MLCCs' degradation

Cite as: Appl. Phys. Lett. **122**, 112902 (2023); doi: 10.1063/5.0138806
Submitted: 14 December 2022 · Accepted: 27 February 2023 ·
Published Online: 13 March 2023



Pedram Yousefian,[a] Shalini Rajpoot, and Clive A. Randall

## AFFILIATIONS

Materials Research Institute, Department of Materials Science and Engineering, Center for Dielectrics and Piezoelectrics, The Pennsylvania State University, University Park, Pennsylvania 16802, USA

**Note:** This paper is part of the APL Special Collection on Energy Conversion and Storage in Functional Dielectrics.
[a]**Author to whom correspondence should be addressed:** pyousefian@psu.edu

## ABSTRACT

The continued development of $BaTiO_3$-based multilayer ceramic capacitors has contributed to further miniaturization by reducing the thickness of each dielectric layer for different voltage range components. MLCC designs that achieve higher volumetric capacitive efficiency must be balanced with stable properties over long operational times at higher fields and temperatures, raising concerns about their reliability. To improve the reliability and slow transient mechanisms of oxygen vacancy electromigration that drive the degradation of insulation resistance of MLCCs, we need to develop new models and improved metrologies to enhance the performance of MLCCs. This paper demonstrates how electrical characterization techniques, such as thermally stimulated depolarization current and highly accelerated life test, can be used to better understand MLCCs' degradation and assess their reliability. Also, the limitations of existing lifetime prediction models and their shortcomings of using mean time to failure in predicting the lifetime of MLCCs are discussed along with future perspectives on evaluating the reliability of MLCCs.



Multilayer ceramic capacitors (MLCCs) are vital passive components packaged in the modern electronics enabling technologies across, from consumer electronics to medical, automotive, and defense applications. MLCCs account for approximately 30% of all components in hybrid circuit modules, whereas ceramic capacitors are more commonly packaged in large arrays below an integrated circuit acting as a power supply to drive the processors. Over 4 trillion MLCC components have been manufactured each year, and over 90% of these have the base metal nickel inner electrodes that are cofired with $BaTiO_3$ based dielectrics.[1]

A typical MLCC component consists of hundreds of layers of dielectric materials that are alternately stacked and separated by parallelly connected internal metal electrodes. In manufacturing of MLCC components, there has been a trend toward further miniaturization to advance Moore's law. The advancement of capacitive volumetric density by reducing the active dielectric layer thickness poses challenges not only in terms of increasing applied electric field through the thinner active dielectric layer but also in terms of electrode uniformity, dielectric compositional dependence, and manufacturing process, all of which affect MLCCs' reliability and lifetime.[2,3] Electrode porosity and roughness, as well as any other external flaws caused by the manufacturing process, can concentrate electric fields and locally enhance electromigration of oxygen vacancies and impact degradation rates.[4–13]

Most commercial high capacitance MLCCs are based on $BaTiO_3$ because of their outstanding dielectric properties such as high permittivity, low dielectric loss, and ability to design properties across broad temperature ranges.[14,15] In cofiring with Ni electrodes, low partial pressure of oxygen is used to prevent the oxidation of Ni. However, under such partial pressures and sintering temperatures, the $BaTiO_3$ system must be in equilibrium with the oxygen reduction reaction, which is given by

$$O_O \rightarrow V_O^{\cdot\cdot} + 2e' + \frac{1}{2}O_2. \quad (1)$$

The non-stoichiometry point defect concentrations are also controlled by partial Schottky reactions, acceptor dopant compensation reactions, and the reduction reaction shown in (1).[16–18] When an electric field is applied, positively charged oxygen vacancies migrate to the cathode via electromigration through ceramic grains, as shown in Fig. 1. Demixing of stoichiometric charge carriers with the oxygen vacancies piling up at grain boundaries and the blocking metal

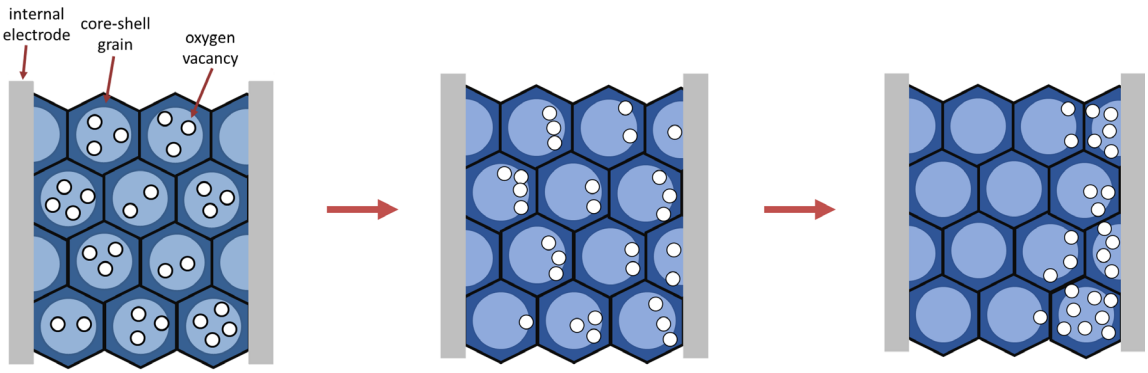


**FIG. 1.** Schematic of oxygen vacancies dynamics and their respective space charge distributions when undergoing the degradation process of MLCCs. Reproduced with permission from Yousefian and Randall, J. Mater. Sci. **57**, 15913 (2022). Copyright 2022 Springer Nature.[21]

electrode causes depression of the Schottky barriers and formation of space charge layers across the dielectric layer. This process gradually degrades the insulation resistance by compromising interfacial Schottky barriers at electrodes and grain boundaries, resulting in an increased leakage current under an electric field and, eventually, thermal or electrical breakdown.[8,19,20]

Thermally stimulated depolarization current (TSDC) is a powerful technique that can be used to analyze relaxation kinetics of polarizable defects and identify various defect mechanisms in insulator materials, including local defect dipole complex changes, local electron trapping, and ionic space charge development both intergranular (ionic charge pileup within individual grains) and transgranular (ionic transportation beyond each grain).[22–28] Figure 2 presents the schematic of typical test conditions for a TSDC experiment. In a TSDC experiment, a sample is

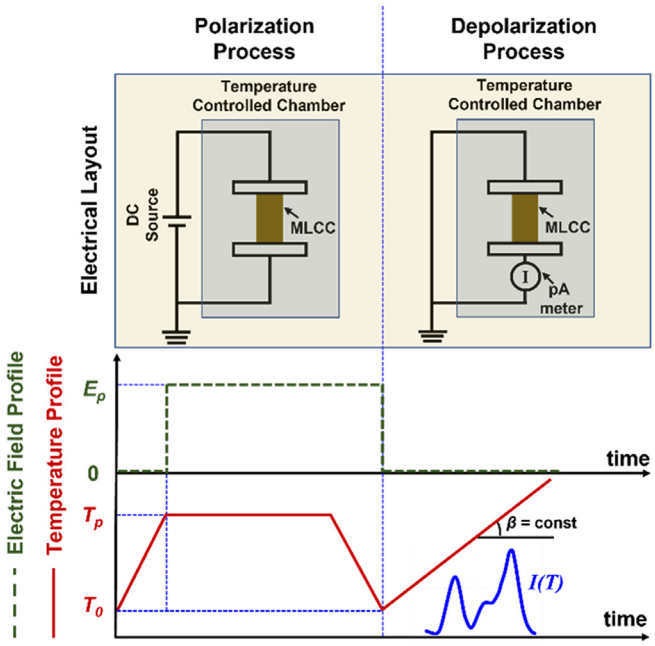


**FIG. 2.** Schematic of typical test conditions for a TSDC experiment.

polarized at a specific temperature $T_p$ under a constant electric field $E_p$ for a period, typically on the order of minutes, creating a metastable state for the defects. The sample was then rapidly cooled to a lower temperature $T_o$, where the polarized defects are frozen. Then, the depolarization occurs with the dielectric being short circuited to a lower temperature $T_o$ and then heating the sample so that each polarization mechanism was in a metastable state, depolarizes to produce a current under constant heating rate ($\beta$), and the leakage current peaks from each depolarization mechanism of the relaxing defects are measured with a PA meter.[29,30]

Figures 3(a) and 3(b) demonstrate the evolution of TSDC peaks in the base metal electrode (BME) X7R MLCC (1206 case size, 1 $\mu$F, and a voltage rating of 50 V) components with increasing heating rate and applied electric field. The heating rate influences the position and shape of TSDC peaks. As the heating rate increases, the TSDC peak narrows and shifts to higher temperatures, as shown in Fig. 3(a). High heating rates accelerate the dipolar interaction process, resulting in a shift of the depolarization currents.[31] The physical origin of each peak can also be determined by studying the temperature dependence of the peak maximum ($T_{max}$) and its dependence on the electric field while heating at a constant rate. When the relaxation current is associated with trapped charges, the $T_{max}$ decreases; when the space charge is the physical origin of the TSDC current, the $T_{max}$ increases.[24,32] Peak A, as shown in Fig. 3(b), is a sharp peak at 125 °C that is independent of $E_p$ and refers to the pyroelectric current associated with the depolarization of the spontaneous dipole alignment at the ferroelectric–paraelectric phase transition of $BaTiO_3$. The $T_{max}$ of peaks B and C increases with increasing of $E_p$, indicating that they are originated from space charge migration in $BaTiO_3$, which are associated with intergranular and transgranular oxygen vacancy electromigration, respectively. These accumulation of oxygen vacancies into metastable ionic space charge regions reduces the reliability of MLCCs by compromising the double Schottky barriers at grain boundaries and electrode interfaces.

Integration of depolarization current peaks and curve fitting will provide important information on the kinetics of relaxational processes such as concentration of mobile charge carriers or dipoles as well as their activation energies. To determine the activation energy of a TSDC peak, three methods are commonly used: the initial rise the full width half maximum of the TSDC peak, and the heating rate dependence of the TSDC peak position.[33] In this study, the third

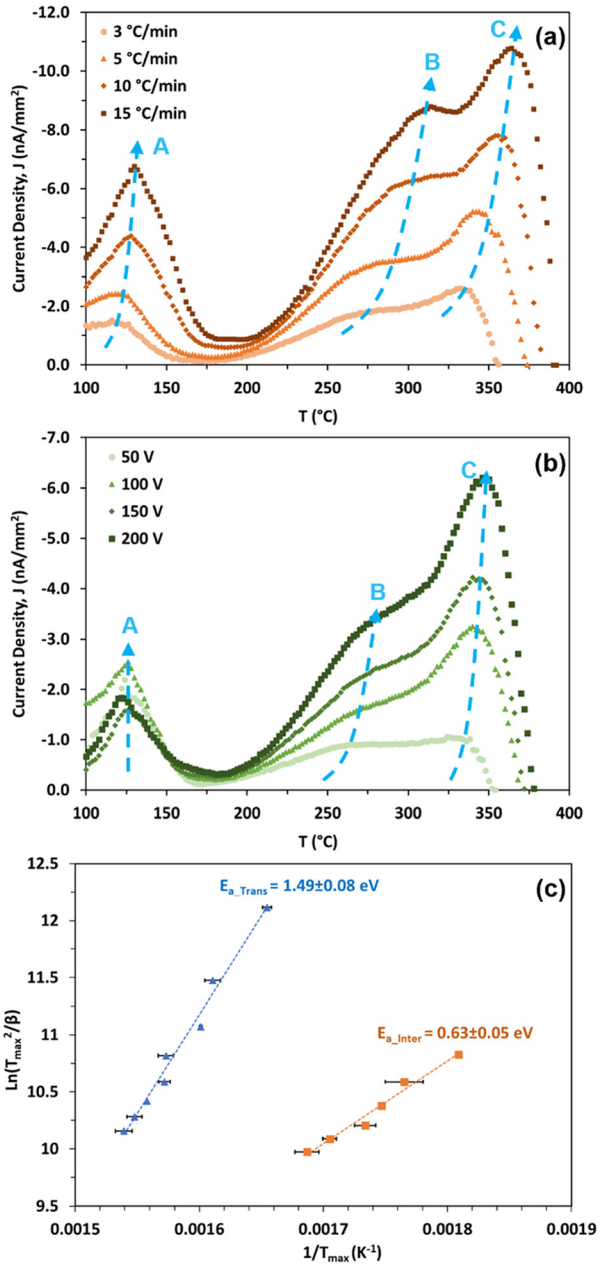


**FIG. 3.** Evolution of TSDC peaks in BME X7R MLCCs (a) with increasing heating rate, samples were poled at 200 °C under a dc bias of 150 V (∼170 kV/cm) for 40 min. (b) With increasing applied voltage bias, samples were poled at 200 °C for 20 min and heated at a rate of 8 °C/min. (c) Estimation of activation energies for the intergranular and transgranular oxygen vacancy relaxation TSDC peaks using a heating rate method.

method was used because deconvolution of TSDC peaks introduced significant error when the first two methods were used. If the temperature dependence of the relaxation time is described by the Arrhenius equation, the activation energy of the TSDC peak can be determined by[34]

$$\ln\left(\frac{T_{\max}^2}{\beta}\right) = \frac{E_a}{kT_{\max}} + \ln\left(\frac{\tau_0 E_a}{k}\right), \tag{2}$$

where $E_a$, $k$, and $\tau_0$ are the activation energy of the barrier height controlling diffusion, Boltzmann's constant, and the relaxation time characteristics, respectively. The activation energies of the transgranular (across grain boundary) and intragranular (in grain) oxygen vacancy relaxation peaks were calculated to be 1.49 ± 0.08 and 0.63 ± 0.05 eV from the slopes of $\ln\left(\frac{T_{\max}^2}{\beta}\right)$ and $\frac{1}{T_{\max}}$ plots, respectively, as shown in Fig. 3(c).

To investigate the overall failure of MLCCs, a highly accelerated life test (HALT) is a traditional method to access the influence of the degradation process and lifetime of MLCCs.[35–41] This is a broadly applicable stress test method that can be used for both development and quality control. In this method, MLCCs are exposed to much higher temperature and voltages than those in normal operating conditions to accelerate the test. The lifetime of MLCCs under normal operating conditions can be extrapolated from the failure time of components, measured by the HALT. A Weibull statistic approach is used to calculate the mean time to failure (MTTF) of MLCCs over a population of components, as shown in Fig. 4. The 2-parameter Weibull distribution function is written as

$$F(t) = 1 - \exp\left(\left(\frac{t}{\eta}\right)^k\right), \tag{3}$$

where t is the failure time, $\eta$ is the scale parameter, and k is a shape parameter corresponding to the slope of the Weibull probability plot.[21,42]

The Eyring model is commonly used to extrapolate HALT results to determine the MTTF of MLCCs in operating conditions, which is expressed as[43]

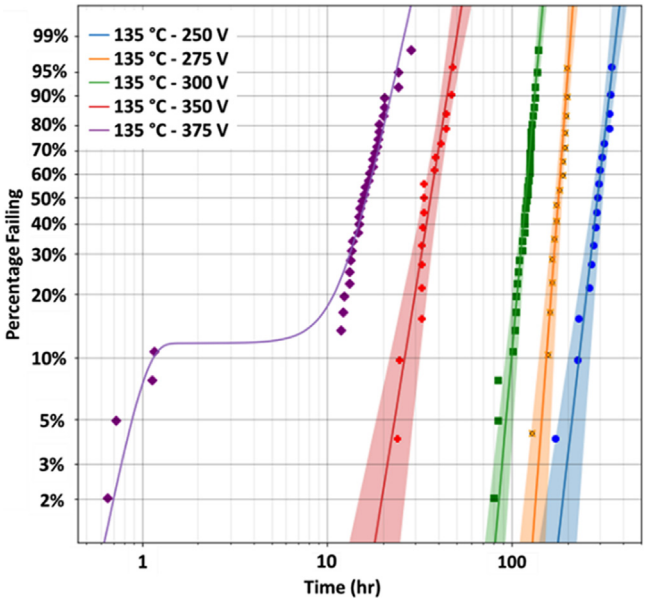


**FIG. 4.** Weibull plot of BME X7R MLCCs under different HALT voltage conditions at 135 °C.

$$\frac{t_1}{t_2} = \left(\frac{V_2}{V_1}\right)^n \exp\left[\frac{E_a}{k_B}\left(\frac{1}{T_1} - \frac{1}{T_2}\right)\right], \tag{4}$$

where $t_1$ and $t_2$ are the MTTFs measured at voltages $V_1$ and $V_2$ at corresponding temperatures $T_1$ and $T_2$, respectively. $n$ and $E_a$ are the electric-field acceleration factor and activation energy of mobility governing the degradation process, respectively. This empirical model has adequate accuracy; however, the factor $n$ is unphysical and varies depending on test conditions.[40,44–46] The $n$ values can be determined using a statistical analysis of a limited number of tests, and these should ideally be constants that are independent of temperature and applied voltage. However, $n$ values are not constant in BME MLCCs, limiting lifetime predictions and necessitating extensive testing to determine the non-linearities of $n$, as shown in Fig. 5(a).

The tipping point lifetime model was developed to address the limitations of the Eyring model, which is based on a physical model that assumes the accumulation of a critical space charge density at the cathode interface and considers local fields. Lifetime of MLCCs in the tipping point model can be predicted as[46,47]

$$t_{crit} = \frac{\rho_{crit}}{a\vartheta Nq}\left[\exp\left(-\frac{E_a}{k_B T}\right)\sinh\left(\frac{qaE_{app}}{2k_B T}\right)\right]^{-1}, \tag{5}$$

where $t_{crit}$ and $\rho_{crit}$ are the predicted lifetime and the critical space charge density at the cathode interface, respectively. Thermally activated jumps between two neighboring sites with the activation energy $E_a$ are considered to be the mechanism of ionic vacancy migration in the bulk crystalline materials; $a$, $\vartheta$, $N$, $q$, and $E_{app}$ are the hopping distance, hopping frequency of the oxygen vacancy, oxygen vacancy concentration, oxygen vacancy charge, and applied electric field, respectively. Based on the following equation:

$$\ln(t) = C(T) - \ln\left(\sinh\left(\frac{\beta' E_{app}}{T}\right)\right), \tag{6}$$

we consider the $\beta'$ as a factor that reflects the local electric field controlling the rate-controlled process of developing the critical ionic space charge within a given microstructure as well as the component design.[29,46] By fitting the failure times data in the ln–ln plot with a slope of $-1$, the values $\beta'$ and $C(T)$ can be defined. The average local field terms arising from the dielectric constant, the electrode roughness, and the average ionic hop distance of an oxygen vacancy in the lattice and across grain boundaries are all included in the $\beta'$ value, which is batch and material dependent but specific to a production batch of MLCC components. The $C(T)$ value is the fitted data's intercept and includes terms such as diffusion activation energy, jump frequency, ionic hop distance, and mobile oxygen vacancy concentration.[47] MTTF data for experimentally processed BME X7R MLCCs under various temperatures and applied electric field conditions were fitted with the Eyring and tipping point models using the linear least

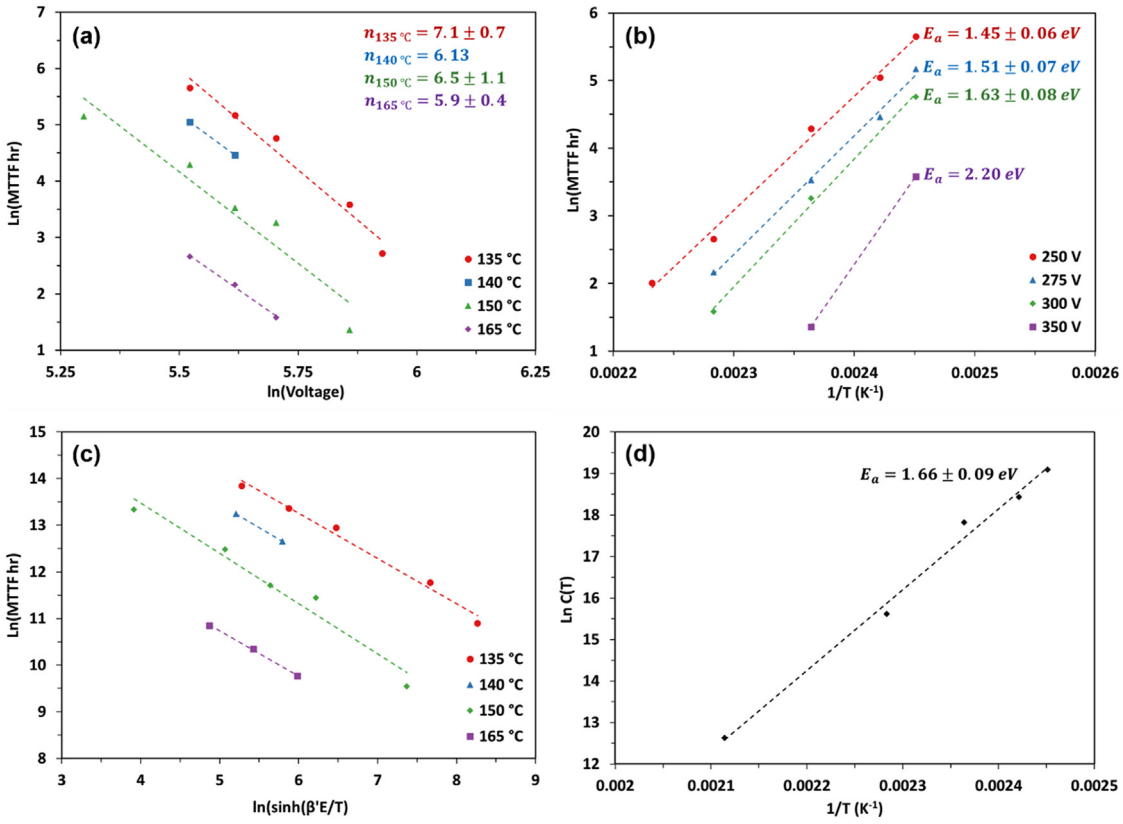


**FIG. 5.** The MTTF data for BME X7R MLCCs were tested under different temperatures and dc bias conditions, and the results were plotted using (a) and (b) the Eyring model and (c) the tipping point model, where datasets are restricted to a single $\beta'$ parameter. (d) Activation energy plot from the driven C(T) values of the tipping point model.

squares regression, presented in Figs. 5(a) and 5(c), respectively. The fitted parameters of the tipping point model are given in Table I. The tipping model appears to be more systematic and predictable across all testing conditions, because the slopes for each MTTF dataset approach −1 when a single $\beta'$ parameter is used; this implies that the failure is caused by a similar mechanism in all samples. It is important to be aware of not overstressing an accelerated lifetime test to extremes that induce multimode failures that are not applicable to the MLCCs under their operating conditions.[8,47]

The activation energy of MLCCs' failures can be determined using the linear slope of the ln(MTTF)–1/T plot in the Eyring model and from slope of the ln(C(T))–1/T plot in the tipping point model, as presented in Figs. 5(b) and 5(d), respectively. The activation energy calculated from the Eyring model varies greatly with applied voltage with an average activation of 1.70 ± 0.30 eV. However, the activation energy calculated by the tipping point model is 1.66 ± 0.09 eV, which has a much smaller standard deviation than the Eyring model. So, the amount of testing for accurate predictions of MTTF could be better served with the tipping model, given its systematic trend and lower errors. Furthermore, the activation energy is comparable to that found in TSDC results for the relaxation peak of transgranular oxygen vacancies, demonstrating that the kinetics of oxygen vacancies' electromigration, particularly transgranular oxygen vacancies' electromigration, is primarily responsible for MLCCs failures. We may expect the depolarization activation energy determined from the TSDC to be slightly less than the initial forward migration, as the grain boundary Schottky barrier height and width may have been compromised under the degradation process. Therefore, for the development of highly reliable MLCCs, it is critical to control microstructural uniformity while emphasizing the blocking effect of grain boundaries against oxygen diffusion.

It is also important to note that in this study, MTTF of MLCCs under different temperatures and dc bias conditions was used to predict the lifetime of MLCCs, which is a common approach among researchers and industries; however, because the failure time data distribution is ignored by the MTTF value, it is unable to fully represent the population of failure times, resulting in inaccurate lifetime predictions and unexpected failures.[21] Therefore, to obtain accurate lifetime predictions, it is necessary to understand the impact of voltage and temperature on failure time distribution, rather than simply considering MTTF values.

In summary, the continued miniaturization of BME MLCCs raises concerns about their reliability by increasing electric field conditions. The presence of oxygen vacancies in BME $BaTiO_3$-based MLCCs is unavoidable due to the low $O_2$ partial pressure sintering conditions of BME MLCCs. The electromigration of oxygen vacancies in the presence of an electric field has a destructive effect on grain boundary Schottky barriers, resulting in insulation resistance degradation and eventually leading to thermal and electrical breakdown of MLCCs. To improve and evaluate the reliability of BME MLCCs, the importance of defect chemistry, microstructural uniformity, and utilization of electrical characterization techniques like TSDC and HALT were discussed. The TSDC technique is an effective method for determining the types of defects that exist in dielectrics and investigating time dependence phenomena that occur during insulation degradation with a focus on electromigration of oxygen vacancies space charge distributions. We demonstrated that the tipping point model is more consistent and accurate across various temperatures and applied electric field conditions. The activation energy calculated from the lifetime prediction models demonstrated that the transgranular oxygen vacancies electromigration is primarily responsible for MLCCs' failures.

**TABLE I.** Fit parameters for the tipping point model measured from Fig. 5(c).

| Temperature (°C) | 135 | 140 | 150 | 165 | 200 |
|---|---|---|---|---|---|
| Slope | −0.91 | −0.93 | −1.01 | −0.91 | −1.24 |
| *C(T)* | 19.09 | 18.43 | 17.82 | 15.62 | 12.63 |

This work was supported by the National Science Foundation, as part of the Center for Dielectrics and Piezoelectrics (CDP) under Grant Nos. IIP-1841453 and IIP-1841466. The authors would like to thank Steven Perini and Jeff Long for their assistance with electrical measurements.

## AUTHOR DECLARATIONS

### Conflict of Interest

The authors have no conflicts to disclose.

### Author Contributions

**Pedram Yousefian:** Writing – original draft (lead); Writing – review & editing (equal). **Shalini Rajpoot:** Writing – review & editing (equal). **Clive A. Randall:** Funding acquisition (lead); Supervision (lead); Writing – review & editing (equal).

## DATA AVAILABILITY

The data that support the findings of this study are available from the corresponding author upon reasonable request.

## REFERENCES

[1]D. Liu, "NASA EEE parts bulletin," Technical Report, Jet Propulsion Laboratory, National Aeronautics and Space Administration, Pasadena, CA, 2013.
[2]S. K. Kurtz, S. Levinson, and D. Shi, J. Am. Ceram. Soc. **72**, 2223 (1989).
[3]K. Hong, T. H. Lee, J. M. Suh, S.-H. Yoon, and H. W. Jang, J. Mater. Chem. C Mater. **7**, 9782 (2019).
[4]K. Jiang, L. Zhang, B. Li, P. Li, S. Yu, R. Sun, Z. Fu, and X. Cao, Ceram. Int. **48**, 30020 (2022).
[5]A. V. Polotai, G.-Y. Yang, E. C. Dickey, and C. A. Randall, J. Am. Ceram. Soc. **90**, 3811 (2007).
[6]G. Y. Yang, E. C. Dickey, C. A. Randall, M. S. Randall, and L. A. Mann, J. Appl. Phys. **94**, 5990 (2003).
[7]M. M. Samantaray, K. Kaneda, W. Qu, E. C. Dickey, and C. A. Randall, J. Am. Ceram. Soc. **95**, 992 (2011).
[8]C. A. Randall and P. Yousefian, J. Eur. Ceram. Soc. **42**, 1445 (2022).
[9]G. Y. Yang, E. C. Dickey, C. A. Randall, D. E. Barber, P. Pinceloup, M. A. Henderson, R. A. Hill, J. J. Beeson, and D. J. Skamser, J. Appl. Phys. **96**, 7492 (2004).
[10]G. Y. Yang, G. D. Lian, E. C. Dickey, C. A. Randall, D. E. Barber, P. Pinceloup, M. A. Henderson, R. A. Hill, J. J. Beeson, and D. J. Skamser, J. Appl. Phys. **96**, 7500 (2004).
[11]T. Sada and N. Fujikawa, Jpn. J. Appl. Phys. **56**, 10PB04 (2017).
[12]J. Yamamatsu, N. Kawano, T. Arashi, A. Sato, Y. Nakano, and T. Nomura, J. Power Sources **60**, 199 (1996).
[13]H. Saito, H. Chazono, H. K. H. Kishi, and N. Y. N. Yamaoka, Jpn. J. Appl. Phys. **30**, 2307 (1991).

[14]S. Trolier-McKinstry and R. E. Newnham, *Materials Engineering* (Cambridge University Press, 2017).
[15]H. Kishi, Y. Mizuno, and H. Chazono, Jpn. J. Appl. Phys., Part 1: Regular Papers Short Notes Rev. Papers **42**, 1 (2003).
[16]S. Lee, C. A. Randall, and Z. K. Liu, J. Am. Ceram. Soc. **91**, 1748 (2008).
[17]N. H. Chan, R. K. Sharma, and D. M. Smyth, J. Am. Ceram. Soc. **65**, 167 (1982).
[18]N. H. Chan and D. M. Smyth, J. Am. Ceram. Soc. **67**, 285 (2006).
[19]T. Baiatu, R. Waser, and K.-H. Hardtl, J. Am. Ceram. Soc. **73**, 1663 (1990).
[20]R. Waser, T. Baiatu, and K. H. Hji, Mater. Sci. Eng., A **109**, 171 (1989).
[21]P. Yousefian and C. A. Randall, J. Mater. Sci. **57**, 15913 (2022).
[22]S.-H. H. Yoon, S.-H. H. Kim, and D.-Y. Y. Kim, J. Appl. Phys. **114**, 074102 (2013).
[23]S. H. Yoon, J. S. Park, S. H. Kim, and D. Y. Kim, Appl. Phys. Lett. **103**, 042901 (2013).
[24]P. Bräunlich, *Thermally Stimulated Relaxation in Solids* (Springer, Berlin Heidelberg, 1979).
[25]A. K. Jonscher, J. Phys. D: Appl. Phys. **24**, 1633 (1991).
[26]S. Takeoka, K. Morita, Y. Mizuno, and H. Kishi, Ferroelectrics **356**, 78–84 (2007).
[27]W. Liu and C. A. Randall, J. Am. Ceram. Soc. **91**, 3251 (2008).
[28]X. Zhang, J. Zhang, Y. Zhou, Z. Xie, Z. Yue, and L. Li, J. Alloys Compd. **662**, 308 (2016).
[29]R. A. Maier, *Dynamics of Oxygen Vacancies and Defect Complexes in the Pervskite Oxide Structure* (The Pennsylvania State University, 2014).
[30]W.-E. Liu, *Impedance/Thermally Stimulated Depolarization Current and Microstructural Relations at Interfaces in Degraded Perovskite Dielectrics* (The Pennsylvania State University, 2009).
[31]A. Torres, J. Jimenez, B. Vega, and J. A. de Saja, Phys. Status Solidi (a) **90**, 749 (1985).
[32]A. K. Jonscher, in *Universal Relaxation Law: A Sequel to Dielectric Relaxation in Solids* (Chelsea Dielectrics Press, London, 1996).
[33]B. Akkopru-Akgun, D. M. Marincel, K. Tsuji, T. J. M. Bayer, C. A. Randall, M. T. Lanagan, and S. Trolier-McKinstry, J. Am. Ceram. Soc. **104**, 5270 (2021).
[34]J. J. M. Ramos and N. T. Correia, Thermochim. Acta **426**, 185 (2005).
[35]B. Dodson and H. Schwab, *Accelerated Testing: A Practitioner's Guide to Accelerated and Reliability Testing* (SAE International, 2006).
[36]A. Teverovsky, "Screening techniques for ceramic capacitors guidelines for selection, screening and qualification of low-voltage commercial multilayer ceramic capacitors for space programs guidelines for selection, screening and qualification of low-voltage commercial," Technical Report, Dell Perot Systems, 2012.
[37]A. Teverovsky, in 2017 IEEE International Reliability Physics Symposium (IRPS), Monterey, California, 2017.
[38]T. Sada, K. Izawa, N. Fujikawa, and Y. Fujioka, Jpn. J. Appl. Phys. **57**, 11UC02 (2018).
[39]D. Liu and M. J. Sampson, in proceedings of CARTS, Jacksonville, FL, 2011.
[40]A. Hernández-López, J. Aguilar-Garib, S. Guillemet-Fritsch, R. Nava-Quintero, P. Dufour, C. Tenailleau, B. Durand, and Z. Valdez-Nava, Materials **11**, 1900 (2018).
[41]R. Confer, J. Canner, T. Trostle, and S. Kurtz, in *41st Electronic Components & Technology Conference* (IEEE, 1991), pp. 320–322.
[42]W. Kuo, W.-T. K. Chien, and T. Kim, *Reliability, Yield, and Stress Burn-In* (Springer US, Boston, MA, 1998).
[43]C. H. Lee and J. R. Yoon, J. Ceram. Process. Res. **23**, 794 (2022).
[44]M. S. Randall, A. S. Gurav, D. J. Skamser, and J. J. Beeson, in *proceedings of CARTS Conference* (Components Technology Institute, Inc., 2003), pp. 134–140.
[45]J.-R. Yoon, K.-M. Lee, and S.-W. Lee, Trans. Electr. Electron. Mater. **10**, 5 (2009).
[46]C. A. Randall, R. Maier, W. Qu, K. Kobayashi, K. Morita, Y. Mizuno, N. Inoue, and T. Oguni, J. Appl. Phys. **113**, 014101 (2013).
[47]K. Morita, T. Shimura, S. Abe, and Y. Konishi, Jpn. J. Appl. Phys. **57**, 11UC03 (2018).